Bulletin of the Seismological Society of America, Vol. 78, No. 6, pp. 2062–2076, December 1988

FINITE-DIFFERENCE CALCULATION OF TRAVEL TIMES

BY JOHN VIDALE

ABSTRACT

The travel times of the first arriving seismic waves through any velocity structure can be rapidly computed on a two- or three-dimensional numerical grid by finite-difference extrapolation from point to point. Wavefronts, rather than the traditional rays, are tracked. Head waves are properly treated and shadow zones are filled by the appropriate diffractions. Differences of less than 0.03 per cent are found between the results of this technique and raytracing for a complex, two-dimensional model. This scheme is useful for the windowing of finite-difference calculations to increase computing speed, and promises to aid in earthquake location, tomographic inversion, and Kirchhoff migration in structures that have strong lateral velocity gradients.

INTRODUCTION

Transit times for seismic waves have been calculated a variety of ways. Generally, more complicated media require more expensive and tricky schemes to find the transit time. If the medium is uniform, the path of seismic waves is the straight line from the source to the receiver, and the travel time is simple to calculate. If the medium is horizontally layered, the path that the energy follows may be derived from the invariance of the ray parameter. The determination of travel times in media that vary laterally as well as vertically has traditionally required some form of raytracing.

Raytracing is based on the concept that seismic energy of infinitely high frequency follows a trajectory determined by the raytracing equations. Physically, these equations describe how energy continues in the same direction until it is refracted by velocity variations. In "shooting" methods of raytracing, a fan of rays is shot from one point in the general direction of the other. The correct path and travel time to connect the two points may then be approached with successively more accurate guesses. Such solutions for two- and three-dimensional media were derived more than 10 years ago (e.g., Julian and Gubbins, 1977, and Cerveny *et al.*, 1977). "Bending" methods of raytracing start with an initial, probably incorrect guess for the ray path. The ray path is bent by a perturbation method until it satisfies a minimum travel-time criterion. Thurber (1987) discusses shooting and bending methods in more detail.

Difficulties with raytracing fall into three categories. First, for strongly varying velocity fields, there can be many paths connecting two points of interest. When there are many paths, it is easy to miss the one with the minimum travel time. Second, if many travel paths to many points are needed, computer costs make the method impractical. Third, even in a smooth medium, there may be a shadow zone, where pairs of points will be connected only by rays that have a very small geometric amplitude because a small change in the take-off angle results in a large change in the ray path. Shooting methods of raytracing often have trouble finding the correct ray in a shadow zone. Bending methods of raytracing do give an answer in shadow zones. However, in both bending and shooting methods it is possible that the answer is only a local minimum, and the global minimum travel time and corresponding ray path remain unknown.

Several approximate methods have been formulated to lessen these problems. Thurber (1981) reduced the three-dimensional problem to two dimensions for economy. Thurber (1983) smoothed the velocity structure to the point where it was practical to compute the ray paths. Um and Thurber (1987) and Prothero *et al.* (1987) presented approximate schemes that work with some realistic velocity structures, but which are still based on raytracing with its inherent limitations.

This note will present a scheme that overcomes all three problems with raytracing. The proposed scheme has already shown its utility in speeding the execution of finite-difference wave-simulation codes and its potential applications to earthquake location, Kirchhoff migration, and tomographic inversion are presented below.

Finite-Difference Travel Time Calculation

The method is outlined in two dimensions for ease of illustration. Extension to three dimensions is simple, but will not be treated here.

The method is formulated for a velocity structure that is sampled at discrete points in two-dimensional space, with equal horizontal and vertical spacing. The question of what continuous velocity structure is implied by the sampled structure is more complicated; for the purpose of testing this scheme, I will compare the results with raytracing where the velocity structure is linearly interpolated between the sampled points. An array of the same dimension as the velocity structure is created to record the travel times. These two arrays use the bulk of the computer memory in this scheme, and the scheme works fastest when the entire program can reside in core.

The source of the seismic waves is assumed to be at grid point A (Figure 1). The timing process is initiated by assigning point A the travel time of zero. The four points adjacent to the point A, labeled B_1 through B_4 in Figure 1, are given the travel times

$$t_i = \frac{h}{2}(s_{Bi} + s_A),$$

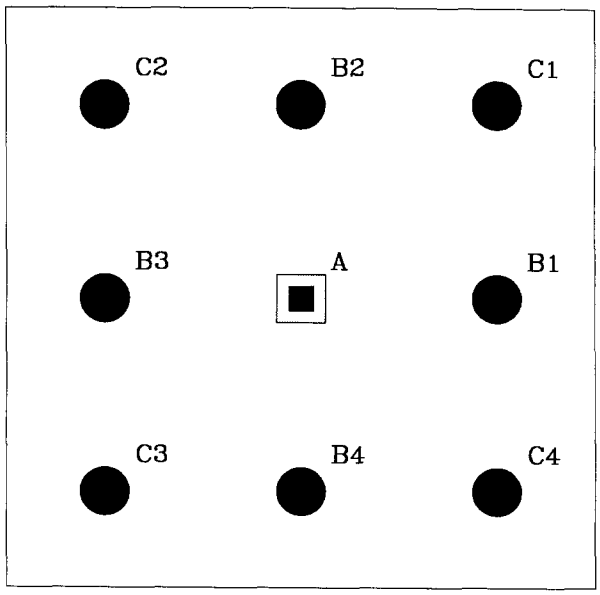

FIG. 1. The source grid point A and the eight points in the ring surrounding point A.

where h is the mesh spacing, s_A is the slowness at the point A, and s_{Bi} is the slowness at the grid point B_i being timed. Next, the travel times for the four corners labeled C_1 through C_4 in Figure 1 are found by the method described below.

I next derive the two formulas that extrapolate the travel times from three corners of a square to the fourth. The first formula will be most accurate for nearly flat wavefronts, the second will be most accurate for strongly curved wavefronts. Consider the geometry in Figure 1 where the travel times between the points $A(t_0)$, $B_1(t_1)$, and $B_2(t_2)$ and the origin are known, and the travel time t_3 between point C_1 and the origin is sought. For the initial calculation, t_0 is zero since it is the travel time of the source grid point, but in general t_0 is not zero and A is not restricted to be the source point.

The propagation of two-dimensional geometric rays and therefore the propagation of two-dimensional wavefronts is guided by the eikonal equation of ray tracing

$$\left(\frac{\partial t}{\partial x}\right)^2 + \left(\frac{\partial t}{\partial z}\right)^2 = s(x, z)^2 \tag{1}$$

that relates the gradient of the travel time to the velocity structure (see, for example, p. 203, Officer, 1974). The co-ordinate axes are x and z, and s is the slowness (inverse of velocity). The two differential terms in equation (1) can be approximated with finite differences as

$$\frac{\partial t}{\partial x} = \frac{1}{2h}(t_0 + t_2 - t_1 - t_3) \tag{2a}$$

and

$$\frac{\partial t}{\partial z} = \frac{1}{2h}(t_0 + t_1 - t_2 - t_3). \tag{2b}$$

Substituting equations (2a) and (2b) into equation (1),

$$t_3 = t_0 + \sqrt{2(hs)^2 - (t_2 - t_1)^2}. \tag{3}$$

Equation (3) gives the travel time to point C1 using the travel times from the source to points A, B1, and B2, in a plane wave approximation. Point A does not need to be the source point for this equation to apply.

The second extrapolation formula assumes locally circular wavefronts. A circular wavefront can be specified by three parameters: (1) the x co-ordinate of the virtual source point, $-x_s$; (2) the z co-ordinate of the virtual source point, $-z_s$; and (3) the origin time for the virtual source t_s. The virtual source point lies at the center of the curvature of the circular wavefronts. For simplicity, the origin of this co-ordinate system is placed at point A, and grid points B1, B2, and C1 have co-ordinates $(h, 0)$, $(0, h)$, and (h, h), respectively. The travel times to points A, B1, and B2 can be expressed as

$$t_0 = t_s + s\sqrt{x_s^2 + z_s^2}, \tag{4a}$$

$$t_1 = t_s + s\sqrt{(x_s + h)^2 + z_s^2}, \tag{4b}$$

and

$$t_2 = t_s + s\sqrt{x_s{}^2 + (z_s + h)^2}. \tag{4c}$$

This system of three equations for the three unknowns t_s, x_s, and z_s can be reduced to a quartic equation in x_s. With knowledge of x_s, z_s, and t_s, t_3 may be calculated from the equation

$$t_3 = t_s + s\sqrt{(x_s + h)^2 + (z_s + h)^2}. \tag{5}$$

The accuracy of the schemes given in equations (3) and (5) may be easily evaluated for the uniform velocity case. The travel times t_0, t_1, and t_2 are computed for a given x_s and z_s, and the t_3 computed with equation (3) or (5) is compared to the correct $t_3{}^c$. Figures 2 and 3 plot the percentage error E, defined by

$$E = \frac{t_3 - t_3{}^c}{hs}$$

where h is the mesh spacing, and s is the slowness, so hs is the travel time between two adjacent grid points. In Figure 2, t_3 is calculated for various x_s and z_s from equation (3), which assumed planar wavefronts. The greatest error appears in the lower left quadrant, which corresponds to the wavefronts with the most curvature. Only strongly curved wavefronts have an error greater than 0.1 per cent.

Figure 3 shows the accuracy of t_3 calculated from equation (5). Since the uniform velocity medium used in Figure 3 only allows circular wavefronts and equation (5) assumes circular wavefronts, the only error will arise from round-off (or faulty computer programming). The test of accuracy shows that errors are uniformly small (on the order of 0.1 per cent) and are particularly small in the region of curved wavefronts. The notable increase in error away from the lower left quadrant in Figure 3 may be partly due to the difficulty of finding the image source from a wavefront with very little curvature. The errors shown in Figure 3 probably indicate the sensitivity of roots to a fourth order equation to round-off error.

For optimal accuracy, one can test whether a plane wavefront is a good approximation from the travel times t_0, t_1, and t_2. If the wavefront is nonplanar, equation (5) gives the best estimate of t_3; if the wavefront seems flat, equation (3) gives a better and quicker answer. I call the combination of equations (3) and (5) the "mixed" scheme. For purposes that require speed but not great accuracy, equation (3) may be used exclusively. I call this the "simple" scheme.

With these schemes to find the time at the fourth corner of a square from the times of the other three corners as a building block, the travel time may be found throughout the grid. First, the times of the four corners (labeled C_1, C_2, C_3, and C_4 in Figure 1) are found from the times of their neighbors. Solution will progress by solving rings of increasing radius around the source point. The source point (radius of 1) and the ring of 8 points (radius of 2) have already been solved.

The inductive scheme for adding a ring of travel times to those already calculated will be described. Consider the ring of radius 5 shown in Figure 4, where all travel times inside the ring are known, but travel times on and outside the ring are unknown. Solution will proceed on the four sides sequentially, followed by the four corner points. I will start arbitrarily with the right side, and find travel times for the points within the rectangular box in Figure 4.

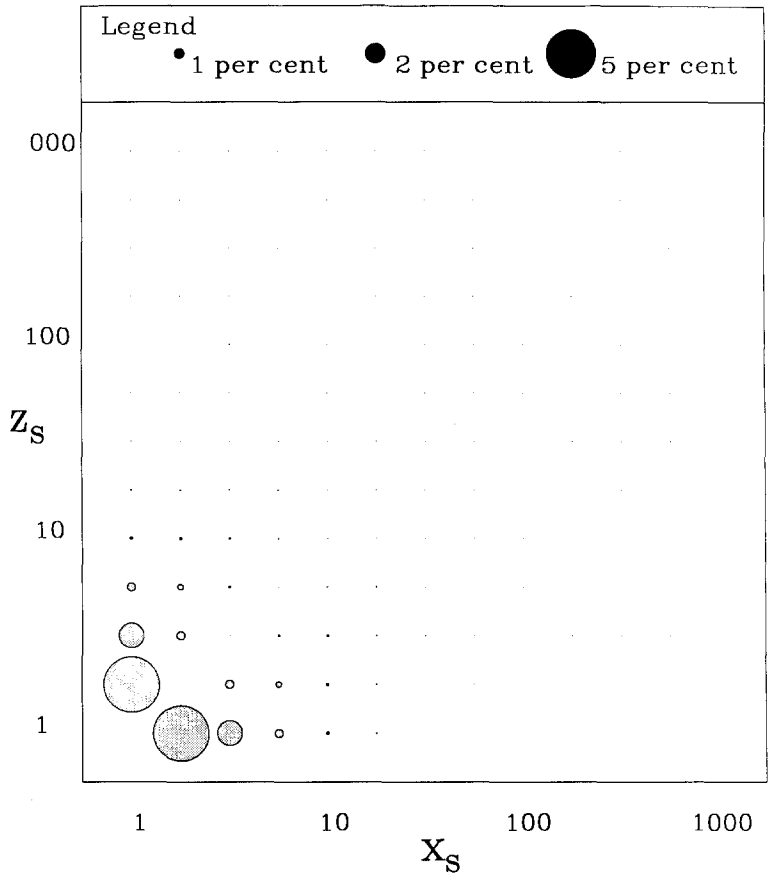

FIG. 2. The accuracy of the extrapolation given by equation (3). The horizontal and vertical coordinates, plotted on log scale, indicate the horizontal and vertical distance to the center of curvature of the wavefront incident on the three points A, B1, and B2. The size of the symbols indicates the error in the extrapolation of travel time to point C1 divided by the hs, where h is the grid spacing and s is the slowness, so the percentage represents the timing error divided by the transit time across the cell.

One may not simply solve for the travel times on a side in order (from top to bottom, for example) because (1) by theory, the solution must follow causality, that is, the time for the part of the ray path leading to a point must be known before the time of the point can be found; and (2) in practice, solving for progressively earlier times along a row results in an instability. An example of the solution of the side of a ring (of radius 8, not 5 as shown in Figure 4) is shown in Figure 5. The points in the row are examined in order from left to right, and the points that are at a relative minimum are identified. A relative minimum is assumed if there is a relative minimum in the time for the adjacent point in the adjacent row that has already been solved in the previous ring. To time the first point on an edge, a noncentered finite-difference of equation (1) must be used. I use the plane-wave formula

$$t_3 = t_0 + \sqrt{(hs)^2 - 0.25(t_2 - t_1)^2}, \tag{6}$$

where t_3 is the time to be found, t_0 is the relative minimum time in the inside row, and t_1 and t_2 are the times on either side of the point whose time is t_0. The accuracy

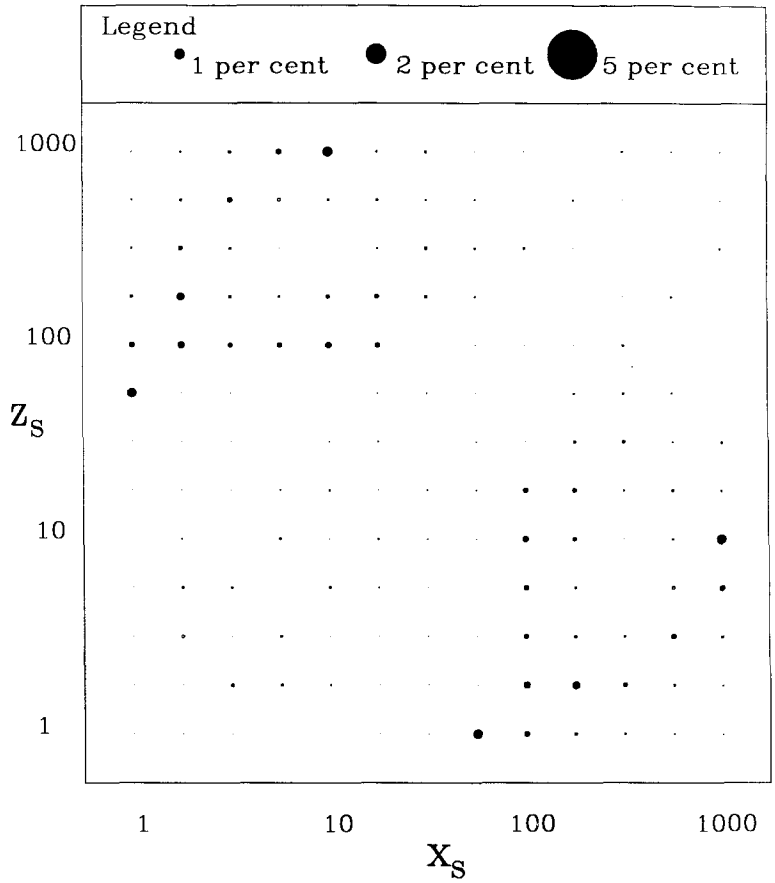

FIG. 3. The accuracy of the extrapolation given solving Equations (4a) through (4c). The horizontal and vertical co-ordinates, plotted on log scale, indicate the horizontal and vertical distance to the center of curvature of the wavefront incident on the three points A, B1, and B2. The size of the symbols indicates the error in the extrapolation of travel time to point C1 divided by the hs, where h is the grid spacing and s is the slowness, so the percentage represents the timing error divided by the transit time across the cell.

of this expression is shown in Figure 6. The image source for Figure 6 will lie near the x-axis because, near a relative minimum in travel time along the column, the ray paths travel nearly horizontally. The accuracy is good along the x-axis.

Starting at each relative minimum point, solution progresses along the row finding the time for each point until the relative maximum is encountered. Upon completion of the left-to-right sweep through the row, the row is swept through in the reverse direction, and the remaining untimed points are solved in order from the relative minima to the relative maxima.

The relative minima are solved from both sides, and the lower of the two estimated travel times is used. This is equivalent to considering two geometric rays coming from either side and only counting the one that arrives first. The neglect of the later arriving of the two possibility simplifies the calculation but results in the loss of all but the first arrival time.

Once the four sides are solved in this way, the times for the corners may be found, and we proceed to the next ring outward. By applying this method iteratively, the entire two-dimensional grid is filled with travel times.

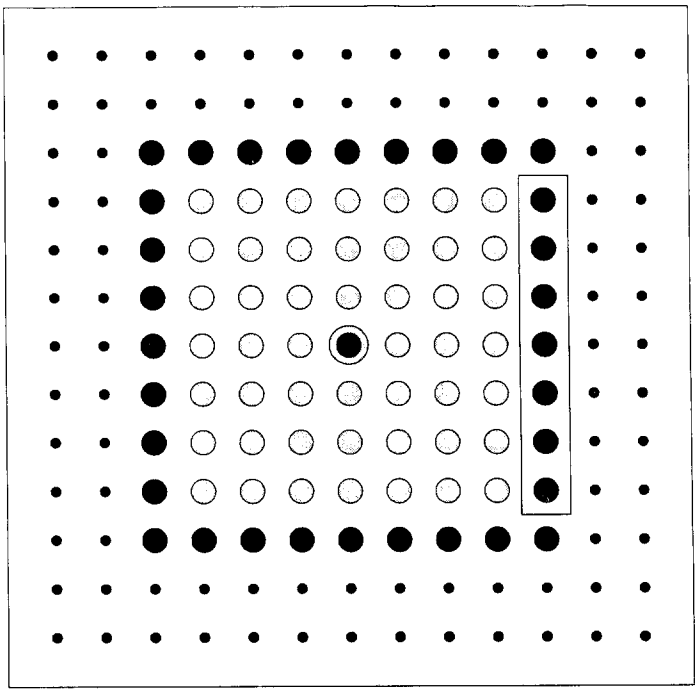

FIG. 4. Picture of the 2-D grid as the numerical calculation of travel time is progressing. The ring of points shown as filled circles are about to be timed. The hollow circles indicate points that have had their travel time calculated. The double circle in the middle shows the source point. The dots are not yet timed, nor will they be timed until the ring of filled circles is done. In the rectangle is a column of points like the one that we will treat in Figure 5.

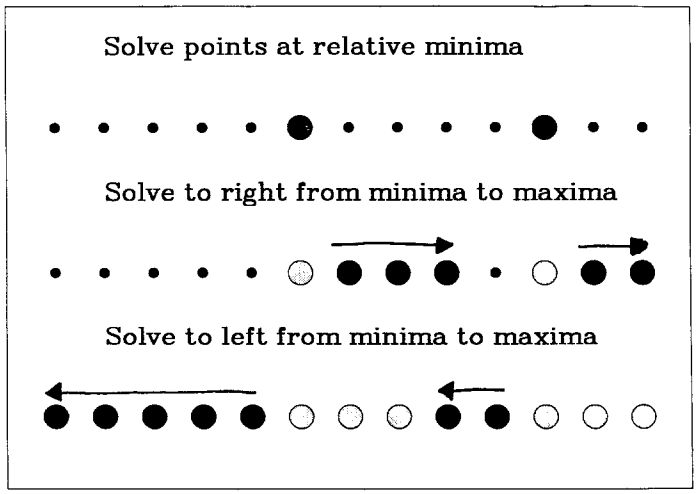

FIG. 5. Sequence of solution of one edge of the ring like that shown in Figure 4. This edge has more points than the edge shown in Figure 4 for clarity of exposition. First, the points that are just outboard of those at a relative minimum are solved by equation (6). Next, we sweep to the right and solve the points from each relative minimum until either a relative maximum or the edge is encountered. Finally, we sweep to the left from each relative minimum until reaching a relative maximum or edge. These three steps will find the times for the entire edge.

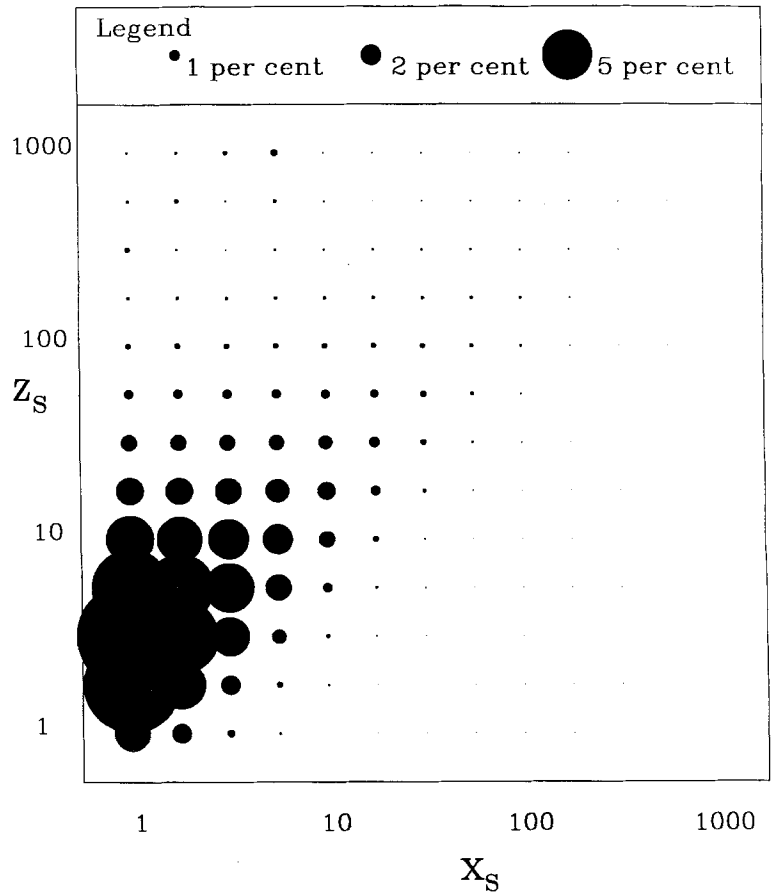

FIG. 6. The accuracy of the extrapolation given by equation (6). The horizontal and vertical coordinates, plotted on log scale, indicate the horizontal and vertical distance to the center of curvature of the wavefront incident on the three points whose timing is known. The size of the symbols indicates the error in the extrapolation of travel time to the fourth point divided by the hs, where h is the grid spacing and s is the slowness, so the percentage represents the timing error divided by the transit time across the cell.

RAYTRACING TEST

Although uniform media are useful for checking accuracy, computing accurate travel times for uniform media is not useful. The most challenging test is the comparison of this finite-difference scheme and a raytracing scheme (from Stork, 1988) for a medium with a strongly varying velocity. The raytracer divides each square of a discretely sampled velocity grid into two triangles each with linear gradients. The ray path across each triangle is the arc of a circle, which may be solved analytically. A random medium with 5 per cent RMS velocity variation is sampled on a grid that has 128 by 128 grid points. The correlation distance is 20 grid points. The velocity variation in this model are shown in Figure 7. The source is placed at the grid point (64, 120), and each of the 128 points at the top surface is a receiver.

The travel times through this structure range from 118 to 136 seconds when a grid spacing of 1 km and mean velocity of 1 km/sec are chosen. The computed

travel times for a uniform velocity and for the variable velocity structure are compared in Figure 8.

Figure 9 shows the differences between the results of the raytracing and the finite-difference calculations using both the mixed scheme [equations (3) and (5)] and the simple scheme [only equation (3)]. The differences would be difficult to see

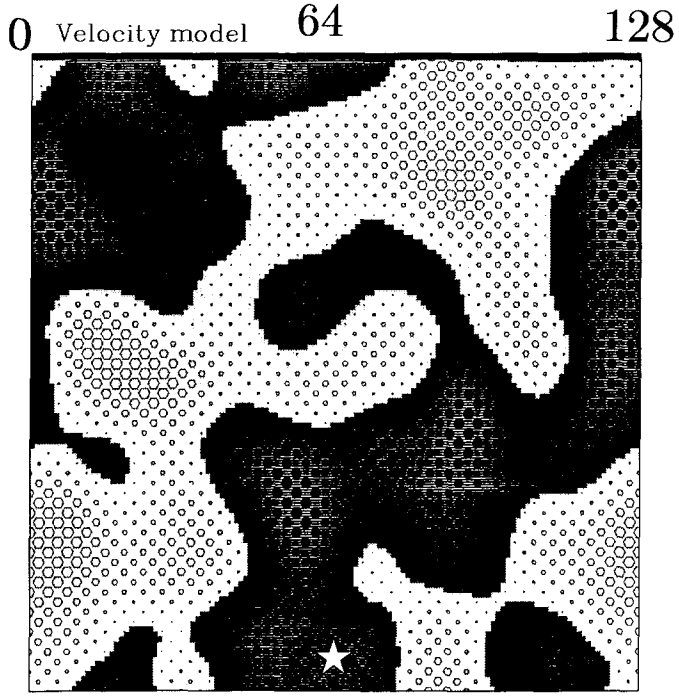

FIG. 7. The velocity model used to compare the finite-difference travel times with the raytracing travel times. Filled circles represent fast velocity, hollow circles show slow velocity, and larger circles indicate more anomalous velocities. The RMS velocity variation is 5 per cent, and the grid has 128 by 128 points, although it is resampled for this figure. The correlation length is 20 grid points. The open star shows the source location, and the heavy line across the top represents the line of 128 receivers.

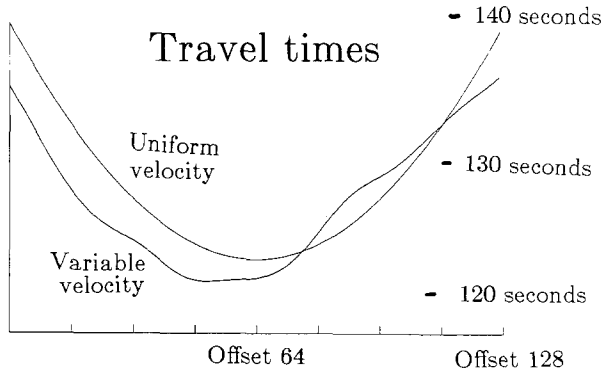

FIG. 8. Comparison of travel times through a medium with a uniform velocity and through the variable velocity medium shown in Figure 7 for the 128 receivers located in Figure 7.

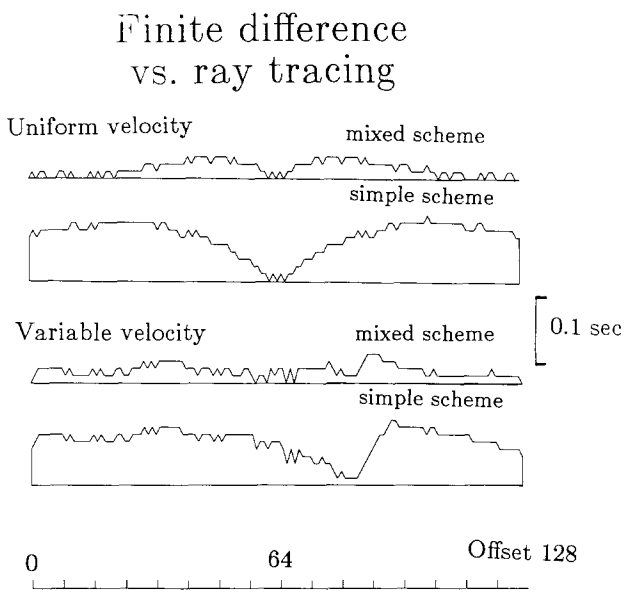

FIG. 9. Differences between raytracing and finite-difference results for the 128 receivers located in Figure 7. The two curves at the top show the differences for a model with a uniform velocity of 1.0 km/sec. The two curves at the bottom are derived with the variable velocity medium shown in Figure 7. The "mixed" scheme applies the finite-difference algorithm when the wavefront is flat, and the circular-wavefront algorithm when it is curved. The "simple" scheme uses the finite-difference algorithm in all cases.

on the scale of Figure 8. The variable velocity field is interpolated with linear gradients by the raytracer and simply averaged by the finite-difference method. The two methods of interpolation do not appear to affect the travel times noticeably, since the differences between the methods for the uniform and variable velocity cases have a similar amplitude and pattern, and the methods of interpolation produce different velocity fields in the variable velocity case but the same field in the uniform case. The differences are close to the round-off error of the single-precision numbers on the computer, as may be seen by the discrete nature of the differences.

In summary, simply using equation (3), the errors are, at most, 0.1 per cent. If the solution to equations (4a), (4b), and (4c) is used when the wavefront is strongly curved, the error is reduced to 0.03 per cent, at most. The accuracy would improve with a finer grid.

Not only is this finite-difference scheme quite accurate, but it found travel times at the four locations for which the powerful raytracer failed, which may be shadow zones, and for one location where the raytracer missed the first arrival and returned a later time. The simple scheme required 30 seconds, the mixed scheme required 90 seconds, while the raytracer required 1800 seconds of CPU time. Also, the finite-difference schemes returned the travel times to all 16,384 (128 times 128) grid points, while the raytracing only returned travel times to the 128 grid points on the surface. The velocity structure of Figure 7 is a complicated and therefore difficult model for raytracing, but it serves to illustrate the simplicity and power of the finite-difference scheme.

APPLICATIONS

Earthquake location. The problem of finding accurate locations for earthquakes in laterally varying structures has inspired many approximate schemes. The original approach was to solve for the set of station corrections that minimize the travel-time residuals from the best-fitting locations for a set of earthquakes (Dewey, 1971). Another approach is to apply station corrections based on delays observed for near-vertical teleseismic arrivals to correct for near-surface as well as deeper laterally varying structures (see Doser and Kanamori, 1986, for example). A third way to reduce the errors that result from not properly considering the effect of laterally varying structure is to put more reliance on nearby stations while using the vertical velocity structure inferred near the earthquake.

The use of raytracing to compute the travel times has been tried with good results for limited sets of earthquakes. The three limitations mentioned above arise, namely, large computer costs, problems with multipathing, and no arrivals in the shadow zones. Perturbation methods and automated searching algorithms can speed the raytracing process (Prothero *et al.*, 1987, Um and Thurber, 1987), and approximations can effectively reduce the calculations to two dimensions (Thurber, 1981).

Still, the process is too slow to allow what the finite-difference calculation allows: the calculation of travel times from each station to the entire volume. A direct search over the entire volume of possible locations is then possible to see which location best fits the observed travel times. A direct search has several advantages; a global minimum to the misfit is assured and the error as a function of location will give a direct estimate of the uncertainty about the best location.

Kirchhoff migration. Kirchhoff migration is a technique used primarily by the oil industry to convert the suite of seismograms from a standard reflection survey into a cross-sectional image of the location of structures that reflect seismic energy (see p. 252 in Yilmaz, 1987, for example). In essence, the energy at each point in time on each seismogram (at each receiver, for each shot), is distributed over all possible scatterers. The possible scatterers form a roughly elliptical surface that is the loci of points where the travel time from the source to the point plus the time from the point to the receiver adds up to the time after the shot the energy is observed.

The scheme thus requires the travel times between all sources and all receivers and every point in space that might have scattered energy. A calculation of this magnitude is beyond the application of raytracing with present computers. If the velocity structure is assumed to be layered, then the travel time is a function only of source or receiver depth (usually zero), scatterer depth, and range to the scatterer, and it no longer depends on absolute horizontal position. In this case, the travel time for every path may be computed simply by the conservation of ray parameter. This is the approach employed by Louie (1987), for example, to examine near-vertical reflectors near Parkfield for a reflection profile that crossed the San Andreas fault.

With the scheme proposed in this note, laterally as well as vertically varying velocity structure may be readily incorporated in such a Kirchhoff inversion. I am investigating this possibility for a fault zone where the velocity structure is known to greatly differ from one side to the other. The amplitude of the first arrival would also be helpful in the Kirchhoff inversion. Since amplitude follows a differential equation similar to equation (1), which relates travel time to velocity, I am also

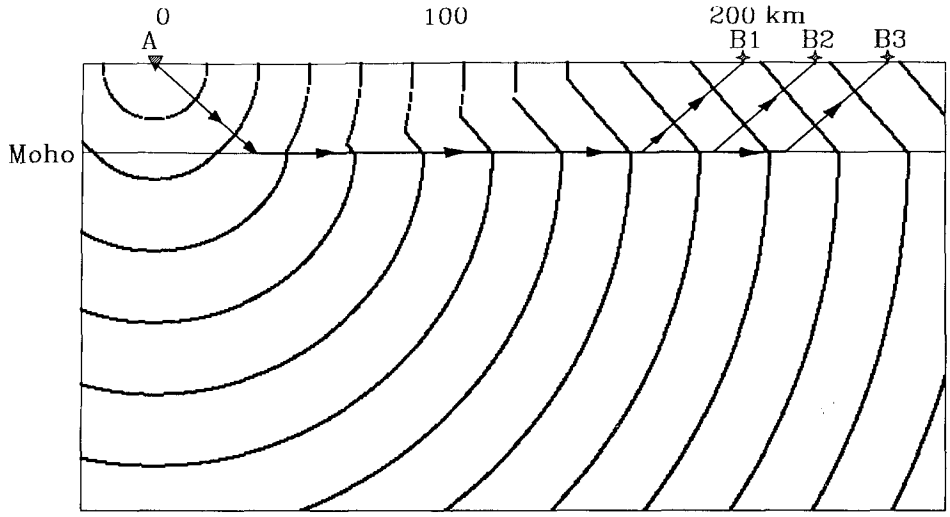

FIG. 10. Location of the wavefront at 3-sec intervals when the source is at the surface of a 30-km thick layer with velocity 6.0 km/sec that is underlain by an 8.0-km/sec half-space. Minimum travel time paths from a source at A to receivers at B1, B2, and B3 are also shown.

considering whether it is feasible to compute the amplitude as well as the travel time on a numerical grid.

Tomographic applications. Once the travel times are computed, the ray paths with the minimum travel time can be found by following the steepest gradient in travel time from the receiver back to the source. These rays are not necessarily geometric rays, since they can also be refractions or diffractions. These types of paths cannot be found by raytracing forward from the source to the receiver, even if the travel times are known. Once a diffraction or refraction branches off from a geometric ray, it can serve as the source for an entire family of geometric rays. This is most easily seen in the familiar case of a refraction along the top of a high-velocity half-space below a low-velocity layer as shown in Figure 10. One rays goes into the refraction, but many rays come out, as shown in Figure 10, and shooting even a fan of rays to find the path along which energy travels from A to B is difficult. Figure 10 also shows a better way to find the path given the travel times; follow the gradient in travel time from B back to A.

Once the timing and ray paths can be found for first arrivals through an arbitrary velocity structure in a routine way, it is easy to set up a tomographic inversion for the velocity structure. It is particularly easy to investigate the resolution and stability of the inversion process. Since first arrivals follow the fastest path, and tomographic inversions mainly use first arrivals, when do the ray paths bunch up in the fast regions and miss some slow regions entirely, and what artifacts appear when a tomographic inversion encounters such problems?

Finite difference speed-up. Knowledge of the travel time to every point in a numerical grid can aid in schemes like finite-difference wave simulation that also use a numerical grid. As Boore (1972) states, there is no need to compute the wave field before the first arrival, since it is uniformly zero. Also, if one is interested only in the first arrivals, there is no need to compute the wave field more than a few seconds behind the first arrival. The finite-difference scheme presented above provides the timing for every point in the grid, which is the information needed to

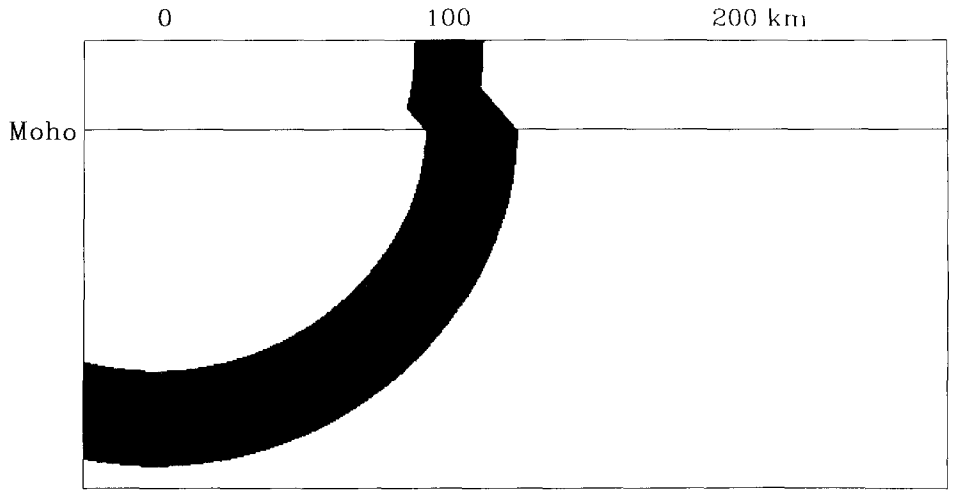

FIG. 11. Window of space that the direct arrival passed through between 13 and 17 seconds after the origin time for the same velocity model as was used for Figure 10.

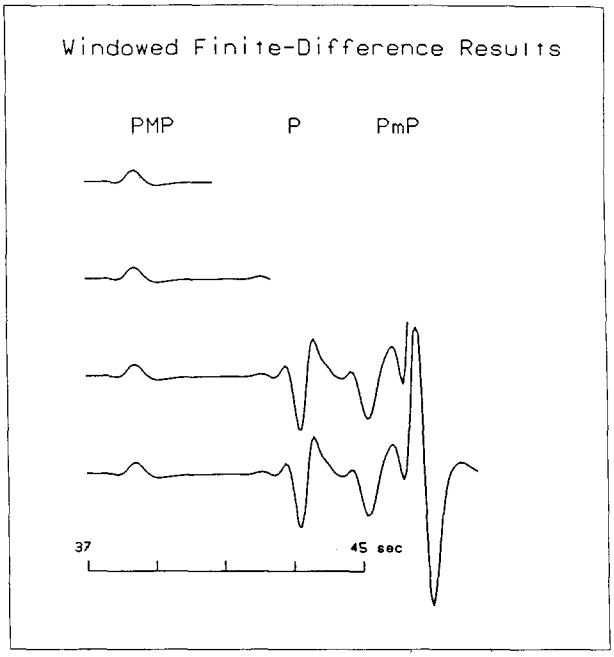

FIG. 12. Comparison of seismograms that result when 3, 5, 9 and 15 seconds behind the wave front are included in the finite-difference calculation. The same velocity model is used as in Figure 10.

turn on the finite-difference calculation just before the first arrival and turn it off after the window of interest.

The cost of including the travel times in finite-difference calculations is the necessity of keeping the travel-time array in memory as well as the three to seven other displacement and media parameter arrays. The additional algebra to keep the finite-difference calculation windowed is negligible. The cost then is a 15 to 40 per cent increase in the memory requirement. The savings from reducing the window

in which the finite-difference calculation is executed typically runs from a factor of three to a factor of 20, depending on the size of the run and the time after the first arrival during which waveforms are desired.

For finite-difference runs simulating *P* and *SH* first arrivals that travel down along slabs (Vidale, 1987), windowing reduces the computer time required by a factor of ten. The cost of producing the travel time field is small compared to that of the finite difference run.

Figure 11 shows the portion of the finite-difference grid that is active 17 seconds after the origin time when a window 4-sec wide is used. The same crustal model is used as above. Only a small fraction of the grid is active at any given time. Figure 12 shows the result of using windows of width 3, 5, 9, and 15 seconds. The three arrivals seen are the diffraction along the Moho (*PMP*), the direct *P* wave in the crust (*P*), and the crustal reverberations, starting with a single reflection off the Moho (*PmP*). From this and other experiments, it is clear that an accurate full-wave solution is computed from the first arrival until the end of the window.

Conclusions

The finite-difference scheme outlined herein is a computationally quick, accurate method to calculate a field of travel times. It may be used in numerous applications, and has several advantages over raytracing methods. Arbitrarily complicated velocity structures may be used. The first arrival is automatically followed and later, multipathed arrivals are ignored. The scheme naturally follows diffractions if they are the first arrivals, even through shadow zones.

Acknowledgments

Support for this work has been provided in part by IGPP-Lawrence Livermore National Laboratory grant 88-37, National Science Foundation grant EAR-8707578, a grant from the W. M. Keck Foundation, and the Institute of Tectonics, University of California, Santa Cruz. Robert W. Clayton made key suggestions. Conversations with Christof Stork helped crystallize this idea. Reviews by David Boore, William Prothero, Stephen Ward, Karen McNally, and especially Heidi Houston elevated the text from the realm of the impenetrable. Contribution Number 47 from the Charles F. Richter Seismological Laboratory at the University of California, Santa Cruz.

References

Boore, D. M. (1972). Finite difference methods for seismic wave propagation in heterogeneous materials, in *Methods of Computational Physics*, vol. 2, B. Alder, S. Fernbach, and M. Rotenberg, Editors, Academic Press, New York, 1–37.

Cerveny, V., I. A. Molotkov, and I. Psencik (1977). Ray methods in seismology, University of Karlova Press, Prague.

Dewey, J. W. (1971). *Seismicity studies with the method of joint hypocentral determination*, Ph.D. Thesis, Massachusetts Institute of Technology, Cambridge, Massachusetts.

Doser, D. I. and H. Kanamori (1986). Depth of seismicity in the Imperial Valley region (1977–1983) and its relationship to heat flow, crustal structure, and the October 15, 1979 earthquake, *J. Geophys. Res.* **91,** 675–688.

Julian, B. R. and D. Gubbins (1977). Three-dimensional seismic ray tracing, *J. Geophys. Res.* **43,** 95–114.

Louie, J. N. (1987). *Seismic reflection experiments imaging the physical nature of crustal structures in southern California*, Ph.D. Thesis, California Institute of Technology, Pasadena, California.

Officer, C. B. (1974). *Introduction to Theoretical Geophysics*, Springer-Verlag, New York.

Prothero, W. A., W. J. Taylor, and J. A. Eickemeyer (1987). A comparison of two fast 3-D raytracers, *EOS* **68,** 1373.

Stork, C. (1988). *Ray trace tomographic velocity analysis of surface seismic reflection data*, Ph.D. Thesis, California Institute of Technology, Pasadena, California.

Thurber, C. H. (1981). *Earth structure and earthquake locations in the Coyote Lake area, central California*, Ph.D. Thesis, Massachusetts Institute of Technology, Cambridge, Massachusetts.

Thurber, C. H. (1983). Earthquake locations and three-dimensional crustal structure in the Coyote Lake area, central California, *J. Geophys. Res.* **88,** 8226–8236.

Thurber, C. H. (1987). Analysis methods of kinematic data from local earthquakes, *Rev. Geofis.* **24,** 793–805.

Um, J. and C. H. Thurber (1987). A fast algorithm for two-point seismic ray tracing, *Bull. Seism. Soc. Am.* **70,** 1137–1148.

Vidale, J. E. (1987). Waveform effects of a high-velocity, subducted slab, *Geophys. Res. Letters* **14,** 542–545.

Yilmaz, O. (1987). *Seismic Data Processing*, S. M. Doherty, Editor, Society of Exploration Geophysicists, Tulsa.

EARTH SCIENCES
APPLIED SCIENCES BUILDING
UNIVERSITY OF CALIFORNIA, SANTA CRUZ
SANTA CRUZ, CALIFORNIA 95064

Manuscript received 27 January 1988